



HAL
open science

Effects of Silane Monolayers on Lysophosphatidylcholine (LysoPC) Detection by Desorption Ionization on Silicon Mass Spectrometry (DIOS-MS) in Solution and Plasma

Antonin Lavigne, Benoît Gilquin, Thomas Gehin, Vincent Jousseume, Marc Veillerot, Yann Chevotot, Magali Phaner-Goutorbe, Christelle Yeromonahos

► To cite this version:

Antonin Lavigne, Benoît Gilquin, Thomas Gehin, Vincent Jousseume, Marc Veillerot, et al.. Effects of Silane Monolayers on Lysophosphatidylcholine (LysoPC) Detection by Desorption Ionization on Silicon Mass Spectrometry (DIOS-MS) in Solution and Plasma. *ACS Applied Materials & Interfaces*, 2023, 15 (15), pp.18685-18693. 10.1021/acsami.3c01181 . hal-04092406

HAL Id: hal-04092406

<https://hal.science/hal-04092406>

Submitted on 9 May 2023

HAL is a multi-disciplinary open access archive for the deposit and dissemination of scientific research documents, whether they are published or not. The documents may come from teaching and research institutions in France or abroad, or from public or private research centers.

L'archive ouverte pluridisciplinaire **HAL**, est destinée au dépôt et à la diffusion de documents scientifiques de niveau recherche, publiés ou non, émanant des établissements d'enseignement et de recherche français ou étrangers, des laboratoires publics ou privés.

This document is confidential and is proprietary to the American Chemical Society and its authors. Do not copy or disclose without written permission. If you have received this item in error, notify the sender and delete all copies.

Effects of Silane Monolayers on Lysophosphatidylcholine (LysoPC) Detection by Desorption Ionization on Silicon Mass Spectrometry (DIOS-MS) from Model Solution and from Blood Plasma

Journal:	<i>The Journal of Physical Chemistry</i>
Manuscript ID	Draft
Manuscript Type:	Article
Date Submitted by the Author:	n/a
Complete List of Authors:	Yeromonahos, Christelle; Ecole Centrale de Lyon, Lavigne, Antonin; Ecole Centrale de Lyon, Gilquin, Benoit; CEA, iRTSV-BGE, ; Université Grenoble Alpes, iRTSV-BGE, Géhin, Thomas; Ecole Centrale de Lyon, Jousseume, Vincent; Laboratoire d'Electronique et de Technologies de l'Information, MINATEC campus Veillerot, Marc; Université Grenoble Alpes, CEA-LETI Chevolot, Yann; CNRS, Phaner-Goutorbe, Magali; Ecole Centrale de Lyon,

SCHOLARONE™
Manuscripts

1
2
3 **Effects of Silane Monolayers on Lysophosphatidylcholine (LysoPC) Detection by**
4
5 **Desorption Ionization on Silicon Mass Spectrometry (DIOS-MS) from Model Solution**
6
7 **and from Blood Plasma**
8
9

10 Antonin Lavigne¹, Benoît Gilquin², Thomas Géhin³, Vincent Jousseume², Marc Veillerot²,
11
12 Yann Chevotot³, Magali Phaner-Goutorbe¹, Christelle Yeromonahos^{1*}
13
14

15
16 ¹ Univ Lyon, Ecole Centrale de Lyon, CNRS, INSA Lyon, Université Claude Bernard Lyon 1,
17
18 CPE Lyon, INL, UMR5270, 69134 Ecully Cedex, France ; ² Univ Grenoble Alpes, CEA,
19
20 LETI, F-38000 Grenoble, France ; ³ Univ Lyon, CNRS, Ecole Centrale de Lyon, INSA Lyon,
21
22 Université Claude Bernard Lyon 1, CPE Lyon, INL, UMR5270, 69134 Ecully Cedex, France
23
24
25

26
27 *** Corresponding Author**
28

29
30 Christelle Yeromonahos: christelle.yeromonahos@ec-lyon.fr, + 33 4 72 18 62 35
31
32
33
34

35 **Abstract**
36

37
38 Desorption ionization on silicon mass spectrometry (DIOS-MS) enables the high throughput
39
40 analysis of low molecular weight biomolecules. However, the detection of metabolites
41
42 biomarkers from complex fluids, like plasma, is subordinated to sample pre-treatments which
43
44 limit clinical applications. Herein, we show that porous silicon chemically modified using
45
46 monolayers of n-propyldimethylmetoxysilane molecules, can be a good candidate for the
47
48 fingerprinting of Lysophosphatidylcholine (LysoPC) in plasma, without any pre-treatment of
49
50 the sample, for DIOS-MS-based diagnosis like sepsis diagnosis. Results are correlated to the
51
52 location of LysoPC molecules inside/outside the pores, determined by time of flight - secondary
53
54 ions mass spectrometry profiling, and to their physico-chemical properties.
55
56
57
58
59
60

1
2
3 **Keywords:** Desorption ionization on silicon mass spectrometry; Silane monolayer; Porous
4
5 silicon; Lysophosphatidylcholine; Blood plasma; Time-of-flight secondary ion spectrometry;
6
7 Sepsis
8
9

10 11 12 13 **Introduction**

14
15
16 Several metabolites, such as amino acids and fatty acids, are biomarkers of a large range of
17
18 inflammatory diseases. Indeed their blood concentrations are highly correlated to the type and
19
20 to the stage of the illness.¹⁻³ Matrix-Assisted Laser Desorption/Ionization Time of Flight Mass
21
22 Spectrometry (MALDI-ToF MS), a soft ionization process, is widely used to detect and analyse
23
24 high molecular weight species with a very high sensitivity, as low as few ng/mL.^{4,5} However,
25
26 in the case of low molecular weight molecules, like metabolites, matrix peaks induce an
27
28 important background noise that can interfere with the analyte peaks and limit their signal-to-
29
30 noise (S/N) ratio. Moreover, to allow MALDI-ToF MS detection of metabolites from blood
31
32 samples, long pre-treatment protocols of blood samples are required to remove abundant high
33
34 molecular weight species. These limitations may induce artefacts and prevent the use of
35
36 MALDI-ToF MS for the rapid detection of blood metabolites, as required for instance in the
37
38 case of sepsis diagnosis.
39
40
41
42
43
44

45 In this context, a set of surface-assisted laser desorption ionization-MS (SALDI-MS) methods,
46
47 which are matrix free strategies, has been developed.⁶ These techniques use the
48
49 nanostructuring of the substrate to desorb and ionize analytes. Even though, for now, no
50
51 consensus has been found on the exact mechanism involved⁷, it is well established that the
52
53 substrates need a strong absorbance in the UV region, a low heat capacity and a reduced thermal
54
55 conductivity to allow the desorption and the ionization of the analytes.⁸ Several type of
56
57 nanostructured substrates, such as gold^{9,10}, silver^{11,12} and alumina^{10,11,13}, have been used in
58
59
60

1
2
3 SALDI-MS due to their optical properties. Carbon-based nanostructure^{14,15} and silicon¹⁶⁻²² have
4
5 also been reported.
6
7

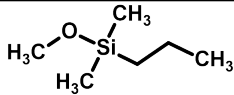
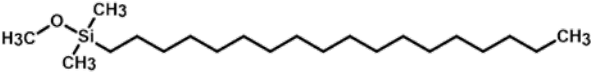
8 Desorption Ionization On Silicon-MS (DIOS-MS), first introduced by Wei et al.²³, is one of
9
10 these technics using the porosity of porous silicon substrate for the ionization of the analytes,
11
12 decreasing drastically the background noise in the metabolite mass range (0-1000 Da) compared
13
14 to MALDI-ToF MS. Also, by tuning the size of the pores, it is possible to sterically exclude
15
16 high molecular weight species from the sample, avoiding long pre-treatment protocols.^{24,25} This
17
18 would, for instance, prevent the need of several solvents for the extraction of high molecular
19
20 weight molecules^{26,27} or the labelling of the analytes of interest with more easily ionisable
21
22 molecules²⁷ for human sample analysis. So, DIOS-MS seems to be promising for the metabolite
23
24 detection in a clinical diagnosis context.
25
26
27

28
29 Silane molecules are widely used to functionalize the surface of bio-analytical devices.²⁸⁻³² In
30
31 addition, silane monolayers allow to prevent from uncontrolled oxidation porous silicon
32
33 surfaces and allow to improve the DIOS-MS limit of detection (LoD) of specific metabolites.³³
34
35 For instance, amino-silane monolayers, with hydrophilic head groups, were shown to be well
36
37 suited for the specific detection of hydrophilic molecules, whereas hydrophobic monolayers
38
39 were shown to improve the detection of any molecules whatever their hydrophobicity.¹⁹ Also,
40
41 Guinan *et al.* have shown that tridecafluoro-1,1,2,2-tetrahydrooctyldimethylchlorosilane (F₁₃)
42
43 onto porous silicon enhances the detection of cocaine and methadone from water, down to
44
45 100ng/mL.¹⁶ Moreover, scarce studies have shown that silanized porous silicon surfaces enable
46
47 the detection of specific metabolites from complex human fluids, without any pre-treatments
48
49 of the sample: a drop of fluid is deposited on the silanized porous silicon surface, high molecular
50
51 weight species are washed from the surface with solvent, and then metabolites are analysed by
52
53 DIOS-MS. In particular, Alhmoud *et al.* have shown, using this protocol, that porous silicon
54
55 surfaces functionalized with F₁₃ allow methadone detection from saliva, urine, and plasma for
56
57
58
59
60

1
2
3 patients treated with this drug.³⁴ Consequently, it is hypothesized that silane monolayers
4 provide a better selective metabolite adsorption, desorption, and/or ionization. Nevertheless, to
5
6 the best of our knowledge, the effects of the alkyl chain length of the silane molecules on the
7
8 DIOS-MS detection of metabolites have never been investigated. Also, even if it is well
9
10 established that the presence of pores is essential to get a DIOS-MS signal, the effects of the
11
12 location of the metabolites (inside the pores or on the surface outside the pores) on the DIOS-
13
14 MS signal have never been studied. Finally, there is only one previous study, the one of
15
16 Alhmould *et al.*, which has shown the possibility to detect a specific metabolite from plasma
17
18 without any pre-treatment of the sample.
19
20
21
22
23

24 Lysophosphatidylcholine (LysoPC) is a biomarker for most of inflammatory diseases that is
25
26 very well detected by mass spectrometry in model solutions.^{1,35} The present study investigates
27
28 the effects of two different silane monolayers on the LysoPC detection by DIOS-MS in solution
29
30 and in plasma. The two silane molecules studied are n-propyldimethylmetoxysilane (named
31
32 CH₃ short in this study) and octadecyldimethylmetoxysilane (named CH₃ long) (**Table 1**).
33
34 Those silane molecules are monovalent, they have different alkyl chain lengths, and they were
35
36 self-assembled in monolayers on porous silicon surfaces (pores of 10 nm in diameter and 1 μm
37
38 in depth). The effects of the silanes monolayers, and of the bare silicon substrate, on the LysoPC
39
40 detection from solution, were correlated both to the chemical properties of LysoPC and to its
41
42 location inside/outside the pores. Then, the possibility of detecting LysoPC, by DIOS-MS, from
43
44 a drop of plasma, using silanized porous silicon substrate without any pre-treatment of the
45
46 sample, is demonstrated.
47
48
49
50
51

52 **Table 1:** Developed formula of the silane molecules used in this study.
53
54
55
56
57
58
59
60

Silane name	Structural formula
CH ₃ short	
CH ₃ long	

1. Material and methods

Chemical and Reagents. Porous silicon substrates were purchased from SiLiMiXT (Tours, France). Pores (10 nm in diameter and 1 μm in depth) were obtained through electrochemical etching of silicon substrates (150mm in diameter, type P, 10-20 mOhms.cm, and 508 μm in thickness). The silane molecules were purchased from ABCR (Karlsruhe, Germany). LysoPC molecules were obtained from Avanti Polar Lipid (reference #855775P). The solvents (tetrahydrofuran 99% (THF), methanol, ethanol and chloroform) and the plasma (reference #P9523-1ml) were obtained from Sigma-Aldrich.

Gas Phase Chemical Surface Functionalization. The porous silicon substrates were cleaned by ozone/ultraviolet treatment at room temperature under an oxygen flow for 30 minutes. Next, the substrates were placed in a vacuum chamber at 150°C for 30 minutes and then allowed to cool at room temperature under nitrogen atmosphere. 100 μL of silane were injected in the reaction chamber and put under vacuum while the temperature was gradually increased to 150°C. After one hour of silanisation, the chamber was pumped for 15 minutes, then the substrates were allowed to cool under nitrogen atmosphere until room temperature was reached. Finally, the samples were washed for 10 minutes in THF and 10 minutes in ultrapure water.

LysoPC preparation. For LysoPC detection in solution, LysoPC was dissolved in a solution of chloroform/methanol (2:1 v/v) at 1 mg/mL. For LysoPC detection in plasma, LysoPC was

1
2
3 spiked in plasma at 50 $\mu\text{g}/\text{mL}$ and 500 $\mu\text{g}/\text{mL}$. Spiked plasma was prepared from a solution of
4
5 LysoPC at 10 mg/mL in chloroform/methanol (2:1 v/v).
6
7

8 **DIOS-MS Analysis.** DIOS mass spectra were obtained using an UltrafleXtreme MALDI-
9
10 TOF/TOF (Bruker Daltonics) equipped with a laser (355 nm). The silicon substrates were held
11
12 on a modified MALDI target plate using copper tape. Ions were detected in reflectron positive
13
14 (RP) or reflectron negative (RN) ion mode at ± 20 kV accelerating potential. The laser was set
15
16 on the large size with a grid voltage of 100 % for RP and RN ion modes. The m/z range was
17
18 10-800 Da. A 1 μL droplet of the solution, or of the spiked plasma, was deposited on the surface
19
20 for 1 min. In the case of the plasma samples, the surface was washed with water, one minute
21
22 after plasma deposition. The washing was done by pipetting 5 μL of ultrapure water on the
23
24 surface. Surface imaging was performed using the FlexImaging 3.0 software (Bruker Daltonics)
25
26 with a spatial resolution of 200 μm (40 spots per droplet in solution and 100 spots per droplet
27
28 in plasma). For each spot, 500-satisfactory laser shots were averaged to obtain a mass spectrum.
29
30 The spectra were analysed using the FlexAnalysis 3.4 software (Bruker Daltonics) for peaks
31
32 detection. The mass spectra of each spot are averaged to determine the peak intensities. To
33
34 evaluate the error bars, spots are randomly divided in two sets, and mass spectra are averaged
35
36 inside each set. The difference in peak intensity between the two half sets of data corresponds
37
38 to the error bars.
39
40
41
42
43
44

45 **Time of flight - secondary ions mass spectrometry (ToF-SIMS) profiling.** High resolution
46
47 mass depth profiles were acquired by ToF-SIMS (ToF-SIMS V from ION-TOF). A bunched
48
49 Bi^{3+} ion gun operation at 15 keV was used as the primary probe for analysis (rastered area 80
50
51 $\times 80 \mu\text{m}^2$). For depth profiling, sputtering was performed using Cs^+ ions at low energy (500 eV,
52
53 rastered area 400 $\times 400 \mu\text{m}^2$). Spectra were normalized using the intensity of the $^{30}\text{Si}^-$ ions in
54
55 the silicon bulk region.
56
57
58
59
60

2. Results and Discussions

LysoPC detection in solution

LysoPC was firstly studied alone in solution, to identify its m/z characteristic peaks in DIOS-MS, and to investigate the effects of silane monolayers on its detection. Firstly, in the absence of matrix, no signal was obtained using non porous substrates (bare silicon, silanized silicon or even the classical stainless steel MALDI target plate).

The spectra obtained in RP ion mode, using the two silanized porous surfaces and the bare porous silicon surface, are presented in **Figure 1**. The relative intensities for each fragment peak are presented in **Table 2**. Only a slight peak is detected at $[M+H]^+$ (524.3 m/z). The main peaks observed correspond to fragments of the molecule at 86.0 m/z , 104.0 m/z , 184.1 m/z , and 198.2 m/z . They are representative of $(CH_3)_3N-CH=CH_2$, choline, phosphocholine, and a phosphocholine-related ion (phosphocholine + CH_2) respectively.³⁶ The main fragment is the one at 86.0 m/z , whatever the surface studied. The silanized surfaces lead to higher intensities, for each fragment peak, than the bare silicon surface. Moreover, the highest intensities are mainly obtained in the case of the CH_3 short monolayer. Indeed the relative intensities for the peaks at 86.0 m/z , 104.0 m/z , 184.1 m/z , and 198.2 m/z are 1, 0.31, 0.18, 0.12 respectively (in the case of the CH_3 short monolayer), 0.77, 0.24, 0.07, 0.17 respectively (in the case of the CH_3 long monolayer), and 0.46, 0.12, 0.17, 0.04 respectively (in the case of the bare silicon substrate).

To explain these results, the location of LysoPC, inside/outside the pores of the three different substrates, was investigated by depth profiling ToF-SIMS analysis of the P^- ion (characteristic of LysoPC, 30.9682 amu) along the pores. Our ToF-SIMS spectra (**Figure 2**) demonstrate a significantly higher intensity of P^- ions inside the pores of the bare silicon substrate and inside the pores functionalized with the CH_3 short monolayer than inside the pores functionalized with the CH_3 long monolayer. This result suggests that the trapping of LysoPC inside the pores improves the effective local and direct ionization of LysoPC molecules, leading to fragment

1
2
3 peaks with high intensity in DIOS-MS analysis. In the case of silicon substrates functionalized
4 with long alkyl chains silane, LysoPC molecules remain outside the pores and are indirectly
5 ionized thanks to the transfer of the laser energy accumulated inside the pores. So, even if the
6 laser energy transfer to the surface is sufficient to get a signal, a higher signal is obtained
7 through local ionization when the molecules are trapped inside the pores. Also, LysoPC is a
8 highly hydrophobic zwitterionic molecule containing two functional groups that are charged at
9 pH 7 (a quaternary ammonium positively charged and a phosphate negatively charged in the
10 phosphocholine side of the molecule), as shown in **Figure 3**. Consequently, it seems reasonable
11 to assume that the positively charged groups of LysoPC will be more easily fragmented when
12 LysoPC is adsorbed on the CH₃ short monolayer than on the negatively charged bare silicon
13 surface, explaining the lower intensity of fragment peaks on the bare silicon surface than on
14 CH₃ short modified porous silicon. On the contrary to fragment peaks, the peak at [M+H]⁺ has
15 a higher intensity on the CH₃ long monolayer and on the bare silicon surface than on the CH₃
16 short monolayer. This result could be explained by an improved desorption of the entire LysoPC
17 molecules outside the pores of hydrophobic substrates (case of CH₃ long monolayer), as well
18 as from the pores of hydrophilic surfaces (case of bare silicone surface), than from the pores of
19 hydrophobic substrates (case of CH₃ short monolayer).
20
21
22
23
24
25
26
27
28
29
30
31
32
33
34
35
36
37
38
39
40
41
42

43 In RN ion mode, depicted in **Figure 4**, no peak is detected at [M-H]⁻ (522.3 m/z). However,
44 several fragments are visible, mainly at 79.0 m/z, 123.1 m/z, 153.1 m/z, and 283.6 m/z. Their
45 relative intensities are presented in **Table 2**. Those peaks correspond to the PO₃⁻, O₃P(CH₂)₂O⁻,
46 CH₃CH(OH)CH₂PH₂O₄⁻, and CH₃(CH₂)₁₆COO⁻ fragments respectively.³⁷ The intensity of these
47 fragments is higher on the CH₃ long monolayer than on the CH₃ short monolayer and on the
48 bare silicon surface. Indeed, the relative intensities of the peaks at 79.0 m/z, 123.1 m/z, 153.1
49 m/z, and 283.6 m/z are 0.28, 0.02, 0.03, 0.01 respectively (in the case of the CH₃ short
50 monolayer), 0.61, 0.08, 0.24, 0.38 respectively (in the case of the CH₃ long monolayer), and
51
52
53
54
55
56
57
58
59
60

1
2
3 0.34, 0.07, 0.04, 0.02 respectively (in the case of the bare silicon substrate). These results
4 suggest that LysoPC trapping inside the pores strongly decreases the detection signal. Thus, it
5 could be more difficult to extract the negatively charged fragments from the pores than the
6 positively charged fragments. Moreover, the larger the fragments, the more difficult it will be
7 to extract them. Indeed, the largest fragment (at 283.6 m/z) is poorly detected on the CH₃ short
8 monolayer (relative intensity 0.01) and on the bare silicon surface (relative intensity 0.02),
9 while the smallest fragment (at 79.0 m/z) is detected (relative intensities 0.28 and 0.34 on CH₃
10 short and on the bare silicon substrate respectively), and the intermediate fragments (at 123.1
11 m/z and 153.1 m/z) are slightly detected (relative intensities 0.02 and 0.03 respectively on CH₃
12 short and 0.07 and 0.04 respectively on the bare silicon substrate).

13
14
15
16
17
18
19
20
21
22
23
24
25
26
27 Consequently, for the detection of LysoPC from a model solution, the CH₃ short and the CH₃
28 long monolayers are more promising than the bare silicon surface, since these monolayers lead
29 to the highest fragment peak intensities (in RP and RN ion mode respectively). Moreover, in
30 model solution, the RP ion mode should be privileged since it allows the detection of LysoPC
31 at [M+H]⁺ contrary to the RN ion mode. However, the RN ion mode allow to decrease the
32 background signal in comparison to the RP ion mode. Consequently, in the following, the RN
33 ion mode was used to investigate the effect of silane monolayers on the detection of LysoPC in
34 plasma.
35
36
37
38
39
40
41
42
43
44
45
46
47
48
49
50
51
52
53
54
55
56
57
58
59
60

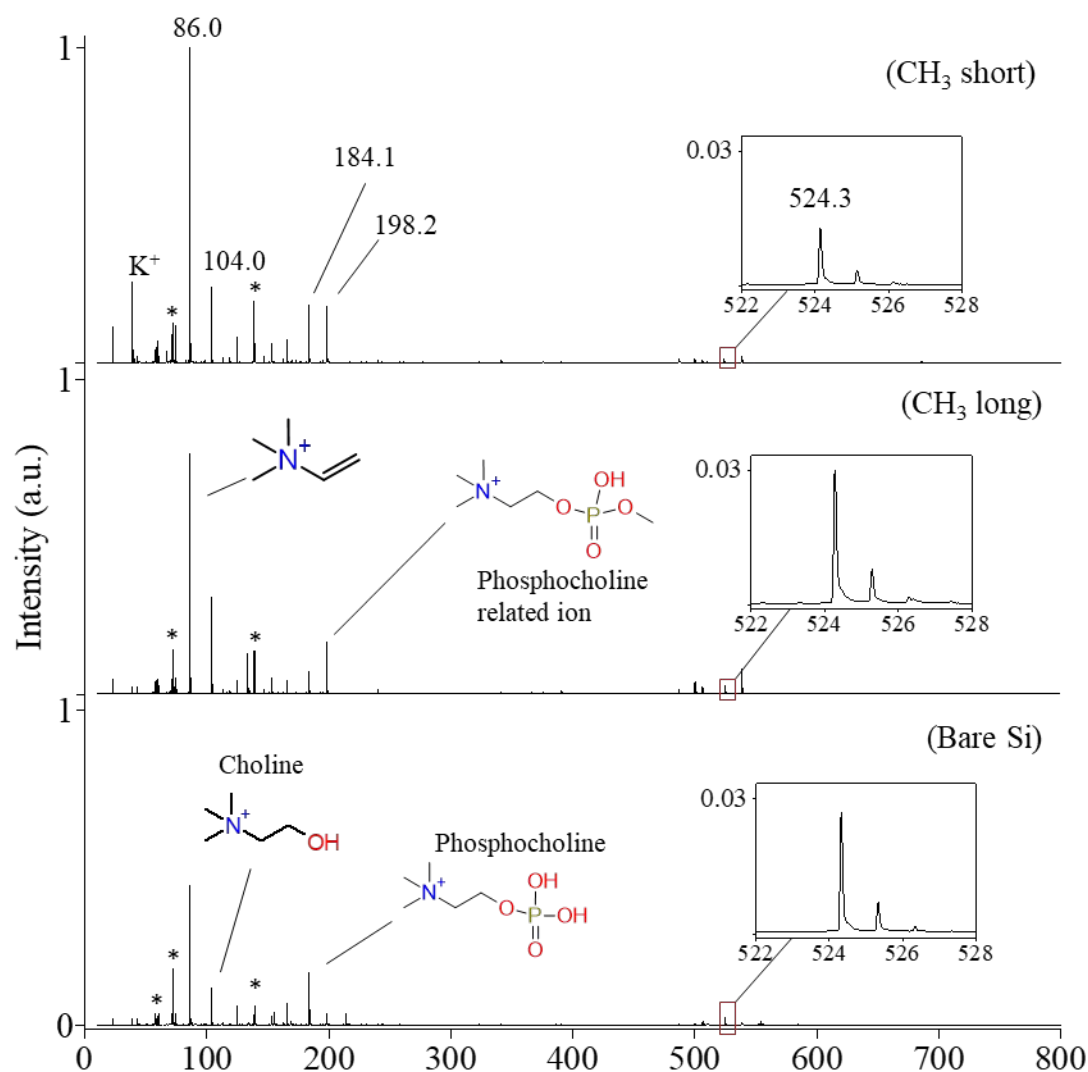


Figure 1: DIOS mass spectra of LysoPC in RP ion mode, alone in solution at 1 mg/mL using the CH₃ short and the CH₃ long monolayers on porous silicon substrates and on the bare porous silicon substrate. The peak of LysoPC is detected at 524.3 m/z and the main fragments (86.0 m/z, 104.0 m/z, 184.1 m/z, and 198.2 m/z) are presented. Peaks corresponding to the substrates are indicated by stars (*). The reference mass spectra of the different surfaces studied, and of the chloroform/methanol solution, without LysoPC, are presented in Supplement Information (**Figures S1-S3**). Total ion current (TIC) normalization is used.

Table 2. Relative intensities of the LysoPC fragment peaks, in RP and RN ion modes, in solution, for the different surfaces studied. Error bars are below 10% (calculated from two half sets of data).

m/z	RP ion mode					RN ion mode			
	86.0	104.0	184.1	198.2	524.3	79.0	123.1	153.1	283.6
CH₃ short	1	0.31	0.18	0.12	0.01	0.28	0.02	0.03	0.01
CH₃ long	0.77	0.24	0.07	0.17	0.03	0.61	0.08	0.24	0.38
bare silicon	0.46	0.12	0.17	0.04	0.02	0.34	0.07	0.04	0.02

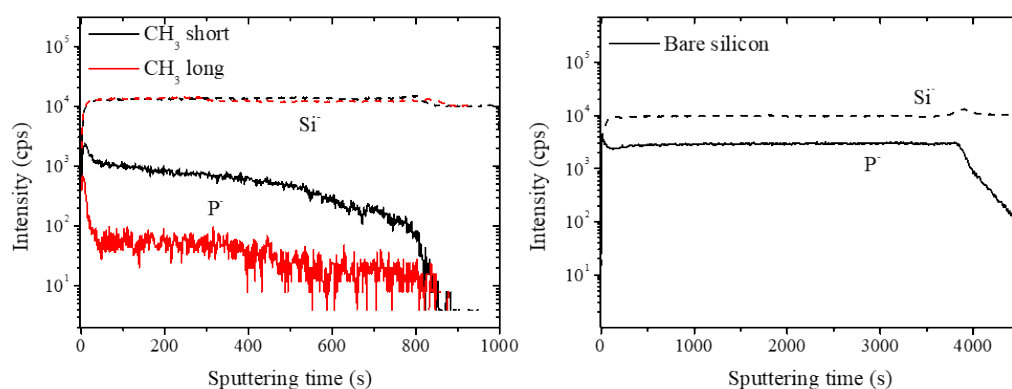
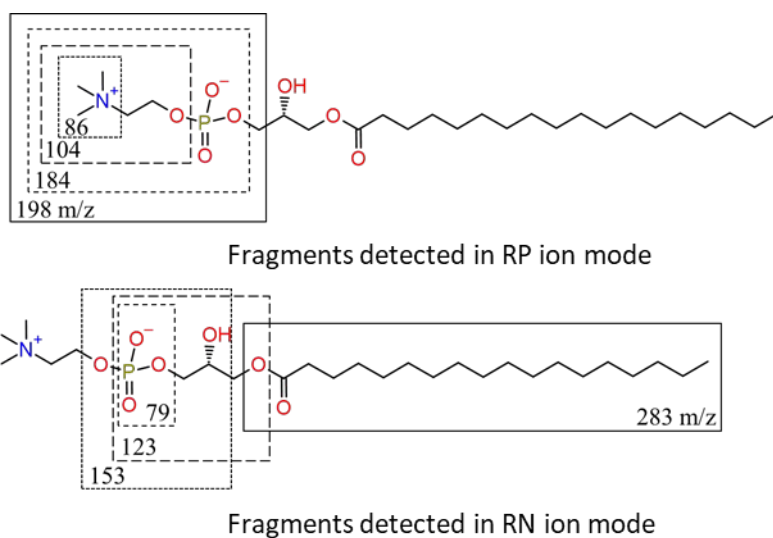


Figure 2. Depth profiling of Si⁻ and P⁻ ions by ToF-SIMS on porous silicon functionalized by CH₃ short and CH₃ long silane monolayers (left), and on bare porous silicon (right). P⁻ ions (30.9682 amu) are specific to the LysoPC molecule. ³⁰Si⁻ in Si bulk is used for normalization.



22 **Figure 3.** Location of the positively and negatively charged fragments of LysoPC detected in
23
24 RP and RN ion mode in DIOS-MS.
25
26
27
28
29
30
31
32
33
34
35
36
37
38
39
40
41
42
43
44
45
46
47
48
49
50
51
52
53
54
55
56
57
58
59
60

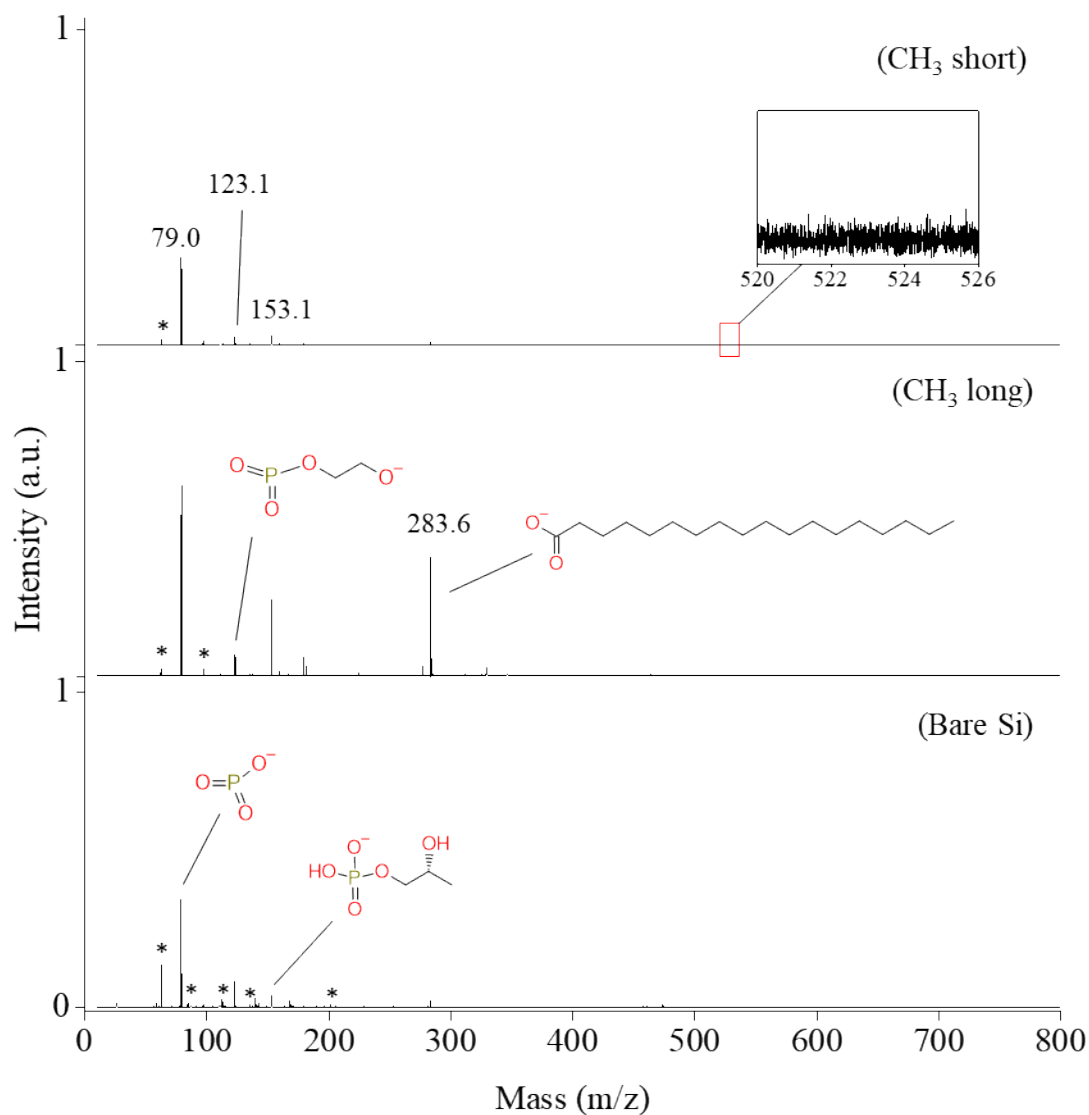


Figure 4. DIOS mass spectra of LysoPC in RN ion mode, alone in solution at 1 mg/mL using the CH₃ short and CH₃ long monolayers on porous silicon substrate and on bare porous silicon substrate. The main fragments (79.0 m/z, 123.1 m/z, 153.1 m/z and 283.6 m/z) are presented. There is no peak of LysoPC at [M-H]⁻ (522.3 m/z). Peaks corresponding to the substrates are indicated by stars (*). The reference mass spectra of the different surfaces studied, and of the chloroform/methanol solution, without LysoPC, are presented in Supplement Information (**Figures S1-S3**). TIC normalization is used.

LysoPC detection from Blood Plasma

1
2
3 LysoPC is present in plasma under physiological conditions at 26 $\mu\text{g}/\text{mL}$.³⁸ To assess its DIOS-
4 MS detection, 50 $\mu\text{g}/\text{mL}$ and 500 $\mu\text{g}/\text{mL}$ of LysoPC were spiked in plasma, and mass spectra of
5 the spiked plasma were compared to the ones of the unmodified plasma. It ensures that the panel
6 of fragments analysed is related to the ones of LysoPC.
7
8
9

10
11
12 Spiked plasma was firstly investigated in RN ion mode, since this mode is expected to yield a
13 lower signal background than the RP ion mode. It should be noted that, after plasma deposition,
14 no peak was detected (**Figure S4**) if the samples were to be analysed as deposited. Several
15 washing protocols were evaluated on the CH₃ short monolayer surface: one, three, and ten water
16 droplets (5 μL) were pipetted one time on the surface (1x1, 3x1, 10x1 protocols) ; two, three,
17 and five water droplets (5 μL) were pipetted five times on the surface (2x5, 3x5, 5x5 protocols)
18 ; and five water droplets (5 μL) were pipetted two times on the surface (5x2 protocol). The
19 normalized intensity of each fragment peak obtained in RN ion mode, for the different washing
20 protocols are presented in **Figures S4-S6**. The 5x5 protocol seems to be the best compromise
21 when considering the intensity improvement of the four fragments. Mass spectra of the spiked
22 plasma on the three different surfaces studied in the RN ion mode, by using the 5x5 washing
23 protocol, are presented **Figure 5**. The relative intensities for each fragment peak are presented
24 in **Table 3**. For all surfaces, no peaks are detected above 300 m/z. Moreover, the CH₃ short
25 monolayer leads to the highest intensity for most of the LysoPC fragments (the relative
26 intensities of the peaks at 79.0 m/z and 123.1 m/z are $2.46 \cdot 10^{-2}$ and $2.50 \cdot 10^{-3}$ respectively on
27 CH₃ short, and $3.28 \cdot 10^{-3}$ and $1.80 \cdot 10^{-3}$ respectively on the bare silicon substrate), except the
28 one at 153.1 m/z that has a slightly higher intensity on the bare porous silicon ($1.52 \cdot 10^{-2}$ on
29 CH₃ short and $2.13 \cdot 10^{-2}$ on the bare silicon substrate). No significant peak was observed on the
30 CH₃ long monolayer. The absence of signal on the CH₃ long monolayer could be explained by
31 the removal of LysoPC molecules, which are mainly outside the pores, during the water
32 washing (using the 5x5 protocol as well as any other protocol). In the case of the CH₃ short
33
34
35
36
37
38
39
40
41
42
43
44
45
46
47
48
49
50
51
52
53
54
55
56
57
58
59
60

1
2
3 monolayer and of the bare silicon surface, LysoPC molecules trapped into the pores are
4
5 protected from washing. Indeed, ToF-SIMS profiling analysis have shown that the presence of
6
7 P^- ions along the pores is not impacted by water washing (**Figure S7**). **Figure 6** presents the
8
9 peaks of LysoPC fragments detected in RN ion mode, in plasma with and without spiking of
10
11 LysoPC (spiking at $50\mu\text{g/mL}$ and at $500\mu\text{g/mL}$) on the CH_3 short monolayer, by using the 5×5
12
13 washing protocol. Same fragments of LysoPC are detected in the spiked plasma as in the
14
15 unmodified plasma, with higher intensity in the spiked plasma. Indeed, the relative intensities
16
17 of the peaks at 79.0 m/z , 123.1 m/z , and 153.1 m/z are 8.00×10^{-2} , 1.61×10^{-2} , 6.59×10^{-2}
18
19 respectively in the $500\mu\text{g/mL}$ spiked plasma, 2.46×10^{-2} , 2.50×10^{-3} , 1.52×10^{-2} respectively in the
20
21 $50\mu\text{g/mL}$ spiked plasma, and 1.13×10^{-2} , 1.67×10^{-3} , 8.61×10^{-3} respectively in the unmodified
22
23 plasma (**Table 4**). These results demonstrate the possibility to detect LysoPC in the unmodified
24
25 plasma sample, by using the CH_3 short monolayer, in RN ion mode. Also, as demonstrated in
26
27 **Figure 5**, no significant peak is observed above 300 m/z and adducts are not detected.
28
29 Nevertheless, a fragment peak attributed to the silane molecules is observed, with high relative
30
31 intensity (5.00×10^{-2} on CH_3 short, and 3.30×10^{-2} on the bare silicon substrate). In the context of
32
33 clinical diagnosis, it could be relevant to maximize the number of LysoPC fragments analysed
34
35 (for sensitivity optimization). Consequently, the possibility to detect LysoPC in RP ion mode
36
37 using the CH_3 short monolayer was investigated. Mass spectra of the unmodified plasma on the
38
39 CH_3 short monolayer in the RP ion mode, by using the 5×5 washing protocol, is presented
40
41 **Figure 7**. The 86.0 m/z and the 184.1 m/z fragments are detected (relative intensities 1.93×10^{-2}
42
43 and 9.88×10^{-3} respectively as shown in **Table 4**). Also, no signal is obtained above 300 m/z ,
44
45 adducts and substrates are not detected. These results demonstrate the possibility to detect
46
47 LysoPC in the unmodified plasma sample, by using the CH_3 short monolayer, both in RP and
48
49 in RN ion modes. This method might be used to detect the drastic decrease in phospholipids
50
51 concentration in case of sepsis diagnosis.
52
53
54
55
56
57
58
59
60

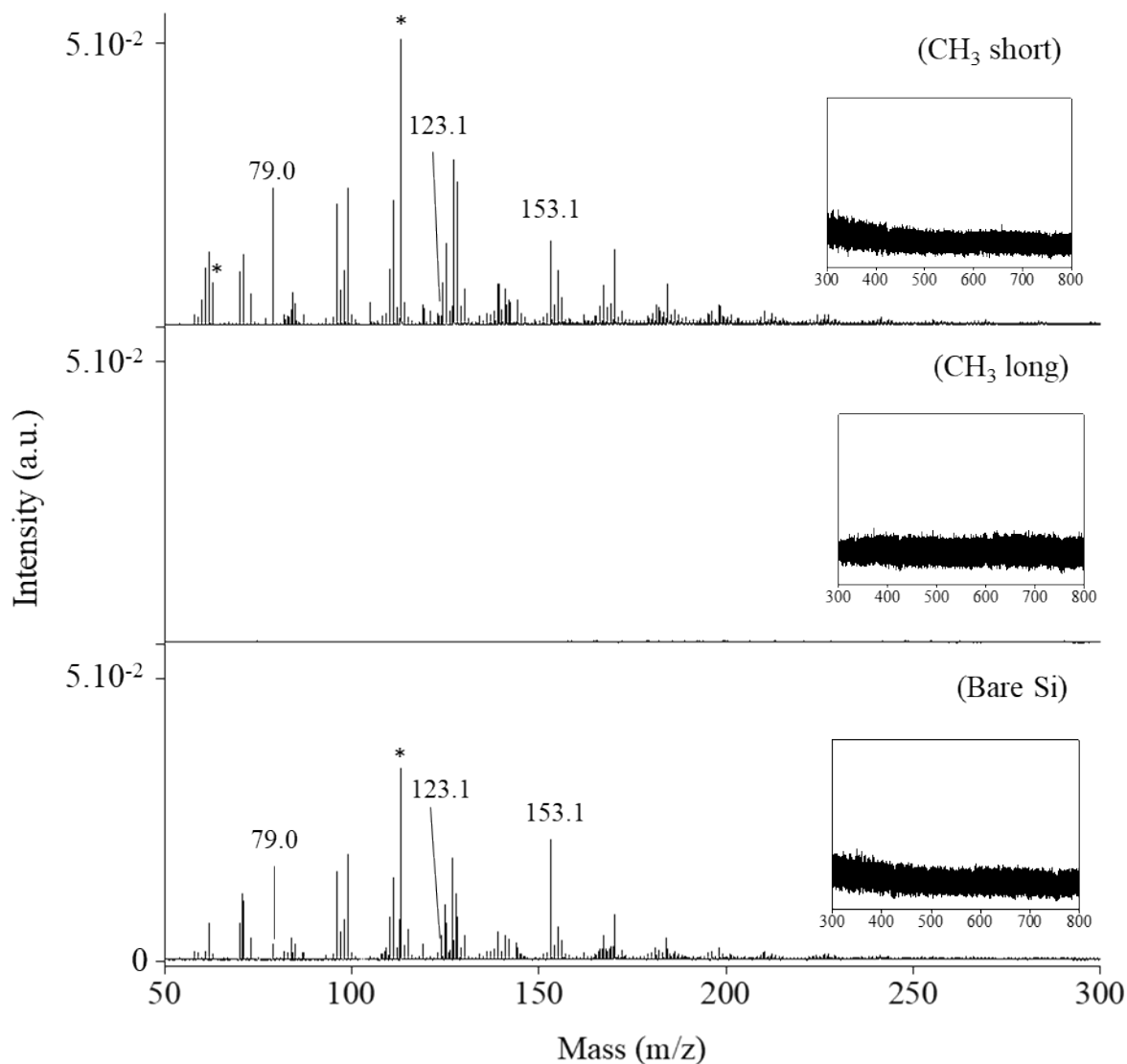


Figure 5. DIOS mass spectra in RN ion mode of plasma spiked with LysoPC (at 50 $\mu\text{g/mL}$) on the CH_3 short and the CH_3 long monolayers, and on the bare silicon. Fragments of LysoPC are indicated (at 79.0, 123.1 and 153.1 m/z). Stars (*) indicate peaks related to the surface. No peaks are observed above 300 m/z . The 5x5 washing protocol is used. The reference mass spectra of the different surfaces studied, and of the chloroform/methanol solution, without

LysoPC, are presented in Supplement Information (**Figures S1-S3**). TIC normalization is used.

Table 3. Relative intensities of the LysoPC fragment peaks, in RN ion mode, in spiked plasma (50 μ g/mL), for the different surfaces studied. No peaks are detected by using CH₃ long, and no peaks are detected at 283.6 m/z. Error bars are below 10% (calculated from two half sets of data). (Spectra are in **Figure 5**)

RN ion mode - spiked plasma (50 μ g/mL)				
m/z	79.0	123.1	153.1	283.6
CH ₃ short	2.46*10 ⁻²	2.5*10 ⁻³	1.52*10 ⁻²	—
CH ₃ long	—	—	—	—
bare silicon	3.28*10 ⁻³	1.80*10 ⁻³	2.13*10 ⁻²	—

Table 4. Relative intensities of the LysoPC fragment peaks, for the CH₃ short monolayer, in RN ion mode in unmodified plasma, in spiked plasma at 50 μ g/mL, in spiked plasma at 500 μ g/mL, and in RP ion mode in unmodified plasma. No peaks are detected at 283.6 m/z in RN ion mode, and no peaks are detected at 104.0 m/z and at 198.2 m/z in RP ion mode. Error bars are below 10% (calculated from two half sets of data). (Spectra are in **Figures 5-7**)

CH ₃ short				
m/z	79.0	123.1	153.1	283.6
RN ion mode – unmodified plasma	1.13*10 ⁻²	1.67*10 ⁻³	8.61*10 ⁻³	—
RN ion mode – spiked plasma (50 μ g/mL)	2.46*10 ⁻²	2.5*10 ⁻³	1.52*10 ⁻²	—
RN ion mode – spiked plasma (500 μ g/mL)	8.00*10 ⁻²	1.61*10 ⁻²	6.59*10 ⁻²	—
m/z	86.0	104.0	184.1	198.2
RP ion mode – unmodified plasma	1.93*10 ⁻²	—	9.88*10 ⁻³	—

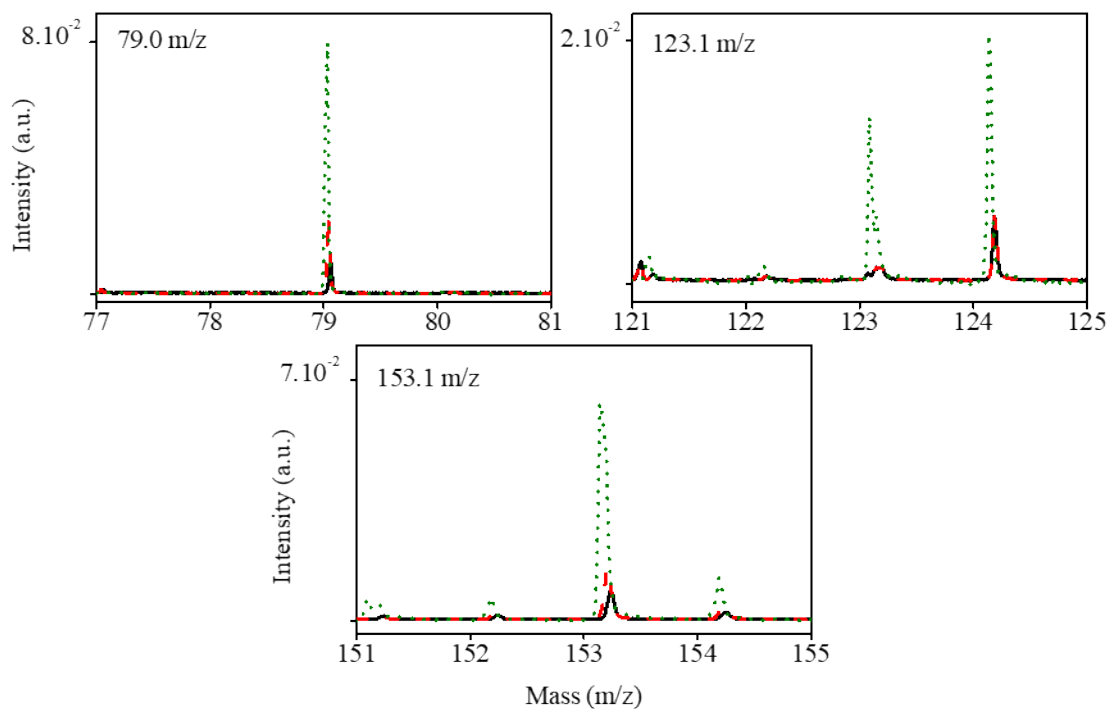
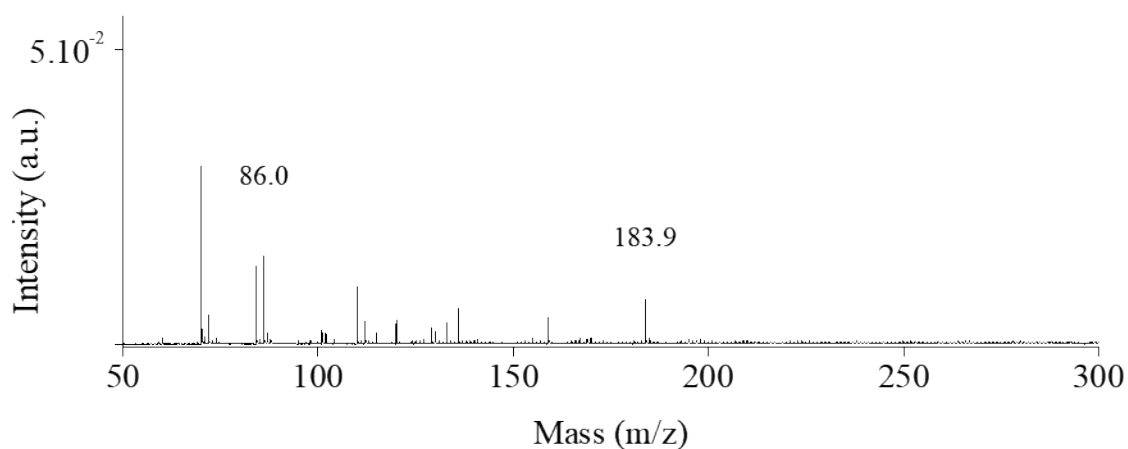


Figure 6. DIOS mass spectra in RN ion mode on the CH_3 short monolayer at (a) 79.0 m/z, (b) 123.1 m/z, and (c) 153.1 m/z, corresponding to fragments of LysoPC. Black solid line corresponds to unmodified plasma, the red long dashed line to the spiked plasma at 50 $\mu\text{g/mL}$, and the green short dashed line to the spiked plasma at 500 $\mu\text{g/mL}$. The 5x5 washing protocol is used. TIC normalization is used.



1
2
3 **Figure 7.** DIOS mass spectra of unmodified plasma on the CH₃ short silane monolayer in RP
4 ion mode. No peaks corresponding to the substrate are detected. TIC normalization is used.
5
6
7
8
9

10 11 **Conclusions**

12
13
14 The DIOS-MS detection of LysoPC, both in solution and in plasma, is demonstrated through
15 the analysis of LysoPC fragments. The use of porous silicon substrate is essential to get a signal.
16 Also, porous silicon substrates chemically modified by silane monolayers lead to higher signal
17 intensity than bare porous silicon substrates.
18
19
20
21
22

23
24 In solution, the signal background, is shown to be lower in RN ion mode than in RP ion mode,
25 both by using chemically functionalized substrates and bare silicon substrates. Moreover, in
26 RN ion mode LysoPC molecules outside the pores are better detected than the ones trapped
27 inside the pores.
28
29
30
31
32

33
34 On the contrary, in plasma, water washing of the surface, after plasma deposition, is required
35 for LysoPC detection. Consequently, only LysoPC molecules trapped inside the pores are
36 detected by DIOS-MS in plasma. Indeed, no signal is obtained by using plane silicon surfaces,
37 or porous surfaces functionalized with long alkyl chain silane monolayers which prevent
38 LysoPC trapping inside the pores, whatever the washing protocols used. The CH₃ short
39 monolayer is demonstrated to be well suited for the detection, in RN ion mode, of LysoPC
40 molecules which are physiologically present in unmodified plasma samples. In addition, this
41 monolayer allows the detection of LysoPC fragments also in RP ion mode. Moreover, the
42 detection does not require any pre-treatment of plasma samples. Thus, porous silicon surfaces
43 functionalized with CH₃ short monolayer could be highly promising for clinical diagnosis of
44 sepsis, an inflammatory disease partly characterized by a drastic decrease in blood
45 phospholipids, in few minutes, from a drop of plasma. Further investigations of the effect of
46
47
48
49
50
51
52
53
54
55
56
57
58
59
60

1
2
3 the different substrates (easily marketable at low cost and high throughput) on the DIOS-MS
4
5 detection of the others blood metabolites specific of sepsis, could lead to the development of a
6
7 platform for clinical diagnosis of sepsis.
8
9

10 Bibliography

- 11
12
13
14 (1) Wang, J.; Sun, Y.; Teng, S.; Li, K. Prediction of Sepsis Mortality Using Metabolite
15
16 Biomarkers in the Blood: A Meta-Analysis of Death-Related Pathways and Prospective
17
18 Validation. *BMC Med.* **2020**, *18* (1), 83. <https://doi.org/10.1186/s12916-020-01546-5>.
19
20
21 (2) Wang, J.; Dong, A.; Liu, G.; Anderson, G. J.; Hu, T. Y.; Shi, J.; Hu, Y.; Nie, G. Correlation
22
23 of Serum Hepcidin Levels with Disease Progression in Hepatitis B Virus-Related Disease
24
25 Assessed by Nanopore Film Based Assay. *Sci. Rep.* **2016**, *6* (1), 34252.
26
27 <https://doi.org/10.1038/srep34252>.
28
29
30 (3) Long, J.; Yang, Z.; Wang, L.; Han, Y.; Peng, C.; Yan, C.; Yan, D. Metabolite Biomarkers
31
32 of Type 2 Diabetes Mellitus and Pre-Diabetes: A Systematic Review and Meta-Analysis.
33
34 *BMC Endocr. Disord.* **2020**, *20* (1), 174. <https://doi.org/10.1186/s12902-020-00653-x>.
35
36
37 (4) Zenobi, R.; Knochenmuss, R. Ion Formation in MALDI Mass Spectrometry. *Mass*
38
39 *Spectrom. Rev.* **1998**, *17* (5), 337–366. [https://doi.org/10.1002/\(SICI\)1098-](https://doi.org/10.1002/(SICI)1098-2787(1998)17:5<337::AID-MAS2>3.0.CO;2-S)
40
41 [2787\(1998\)17:5<337::AID-MAS2>3.0.CO;2-S](https://doi.org/10.1002/(SICI)1098-2787(1998)17:5<337::AID-MAS2>3.0.CO;2-S).
42
43
44 (5) Dreisewerd, K. The Desorption Process in MALDI. *Chem. Rev.* **2003**, *103* (2), 395–426.
45
46 <https://doi.org/10.1021/cr010375i>.
47
48
49 (6) Sunner, J.; Dratz, E.; Chen, Y.-C. Graphite Surface-Assisted Laser Desorption/Ionization
50
51 Time-of-Flight Mass Spectrometry of Peptides and Proteins from Liquid Solutions. *Anal.*
52
53 *Chem.* **1995**, *67* (23), 4335–4342. <https://doi.org/10.1021/ac00119a021>.
54
55
56 (7) Müller, W. H.; Verdin, A.; De Pauw, E.; Malherbe, C.; Eppe, G. Surface-assisted Laser
57
58 Desorption/Ionization Mass Spectrometry Imaging: A Review. *Mass Spectrom. Rev.*
59
60 **2022**, *41* (3), 373–420. <https://doi.org/10.1002/mas.21670>.

- 1
2
3 (8) Picca, R. A.; Calvano, C. D.; Cioffi, N.; Palmisano, F. Mechanisms of Nanophase-Induced
4 Desorption in LDI-MS. A Short Review. *Nanomaterials* **2017**, *7* (4), 75.
5
6 <https://doi.org/10.3390/nano7040075>.
7
8
9
10 (9) Duan, J.; Wang, H.; Cheng, Q. On-Plate Desalting and SALDI-MS Analysis of Peptides
11 with Hydrophobic Silicate Nanofilms on a Gold Substrate. *Anal. Chem.* **2010**, *82* (22),
12 9211–9220. <https://doi.org/10.1021/ac102262m>.
13
14
15
16 (10) Fournelle, F.; Yang, E.; Dufresne, M.; Chaurand, P. Minimizing Visceral Fat
17 Delocalization on Tissue Sections with Porous Aluminum Oxide Slides for Imaging Mass
18 Spectrometry. *Anal. Chem.* **2020**, *92* (7), 5158–5167.
19
20 <https://doi.org/10.1021/acs.analchem.9b05665>.
21
22
23 (11) Baquer, G.; Sementé, L.; García-Altres, M.; Lee, Y. J.; Chaurand, P.; Correig, X.; Ràfols,
24 P. RMSIcleanup: An Open-Source Tool for Matrix-Related Peak Annotation in Mass
25 Spectrometry Imaging and Its Application to Silver-Assisted Laser Desorption/Ionization.
26 *J. Cheminformatics* **2020**, *12* (1), 45. <https://doi.org/10.1186/s13321-020-00449-0>.
27
28
29 (12) Lauzon, N.; Dufresne, M.; Chauhan, V.; Chaurand, P. Development of Laser Desorption
30 Imaging Mass Spectrometry Methods to Investigate the Molecular Composition of Latent
31 Fingermarks. *J. Am. Soc. Mass Spectrom.* **2015**, *26* (6), 878–886.
32
33 <https://doi.org/10.1007/s13361-015-1123-0>.
34
35
36 (13) Kuwata, K.; Itou, K.; Kotani, M.; Ohmura, T.; Naito, Y. DIUTHAME Enables Matrix-free
37 Mass Spectrometry Imaging of Frozen Tissue Sections. *Rapid Commun. Mass Spectrom.*
38 **2020**, *34* (9). <https://doi.org/10.1002/rcm.8729>.
39
40
41 (14) Kim, Y.-K.; Na, H.-K.; Kwack, S.-J.; Ryoo, S.-R.; Lee, Y.; Hong, S.; Hong, S.; Jeong, Y.;
42 Min, D.-H. Synergistic Effect of Graphene Oxide/MWCNT Films in Laser
43 Desorption/Ionization Mass Spectrometry of Small Molecules and Tissue Imaging. *ACS*
44 *Nano* **2011**, *5* (6), 4550–4561. <https://doi.org/10.1021/nn200245v>.
45
46
47
48
49
50
51
52
53
54
55
56
57
58
59
60

- 1
2
3 (15) Abdelhamid, H. N.; Wu, H.-F. A Method to Detect Metal–Drug Complexes and Their
4 Interactions with Pathogenic Bacteria via Graphene Nanosheet Assist Laser
5 Desorption/Ionization Mass Spectrometry and Biosensors. *Anal. Chim. Acta* **2012**, *751*,
6 94–104. <https://doi.org/10.1016/j.aca.2012.09.012>.
7
8
9
10
11
12 (16) Guinan, T.; Ronci, M.; Vasani, R.; Kobus, H.; Voelcker, N. H. Comparison of the
13 Performance of Different Silicon-Based SALDI Substrates for Illicit Drug Detection.
14 *Talanta* **2015**, *132*, 494–502. <https://doi.org/10.1016/j.talanta.2014.09.040>.
15
16
17
18
19 (17) Budimir, N.; Blais, J.-C.; Fournier, F.; Tabet, J.-C. The Use of Desorption/Ionization on
20 Porous Silicon Mass Spectrometry for the Detection of Negative Ions for Fatty Acids.
21 *Rapid Commun. Mass Spectrom.* **2006**, *20* (4), 680–684.
22
23
24
25
26
27
28
29 (18) Jemere, A. B.; Bezuidenhout, L. W.; Brett, M. J.; Harrison, D. J. Matrix-Free Laser
30 Desorption/Ionization Mass Spectrometry Using Silicon Glancing Angle Deposition
31 (GLAD) Films: Matrix-Free LDI-MS Using Silicon GLAD Films. *Rapid Commun. Mass*
32 *Spectrom.* **2010**, *24* (15), 2305–2311. <https://doi.org/10.1002/rcm.4634>.
33
34
35
36
37
38 (19) Trauger, S. A.; Go, E. P.; Shen, Z.; Apon, J. V.; Compton, B. J.; Bouvier, E. S. P.; Finn,
39 M. G.; Siuzdak, G. High Sensitivity and Analyte Capture with Desorption/Ionization Mass
40 Spectrometry on Silylated Porous Silicon. *Anal. Chem.* **2004**, *76* (15), 4484–4489.
41
42
43
44
45
46
47 (20) Zhou, Y.; Peng, C.; Harris, K. D.; Mandal, R.; Harrison, D. J. Salt Segregation and Sample
48 Cleanup on Perfluoro-Coated Nanostructured Surfaces for Laser Desorption Ionization
49 Mass Spectrometry of Biofluid Samples. *Anal. Chem.* **2017**, *89* (6), 3362–3369.
50
51
52
53
54
55
56 (21) Dupré, M.; Enjalbal, C.; Cantel, S.; Martinez, J.; Megouda, N.; Hadjersi, T.; Boukherroub,
57 R.; Coffinier, Y. Investigation of Silicon-Based Nanostructure Morphology and Chemical
58
59
60

- 1
2
3 Termination on Laser Desorption Ionization Mass Spectrometry Performance. *Anal.*
4
5 *Chem.* **2012**, *84* (24), 10637–10644. <https://doi.org/10.1021/ac3021104>.
6
7
8 (22) Singh, R.; Bezuidenhout, L. W.; Jemere, A.; Wang, Z.; Brett, M.; Harrison, D. J.
9
10 Engineering Matrix-Free Laser Desorption Ionization Mass Spectrometry Using Glancing
11
12 Angle Deposition Films: Matrix-Free LDI Using GLAD Films. *Rapid Commun. Mass*
13
14 *Spectrom.* **2017**, *31* (7), 631–638. <https://doi.org/10.1002/rcm.7826>.
15
16
17 (23) Wei, J.; Buriak, J. M.; Siuzdak, G. Desorption–Ionization Mass Spectrometry on Porous
18
19 Silicon. *Nature* **1999**, *399* (6733), 243–246. <https://doi.org/10.1038/20400>.
20
21
22 (24) Bouamrani, A.; Hu, Y.; Tasciotti, E.; Li, L.; Chiappini, C.; Liu, X.; Ferrari, M.
23
24 Mesoporous Silica Chips for Selective Enrichment and Stabilization of Low Molecular
25
26 Weight Proteome. *PROTEOMICS* **2010**, *10* (3), 496–505.
27
28 <https://doi.org/10.1002/pmic.200900346>.
29
30
31 (25) Wang, X.; Teng, F.; Wang, Y.; Lu, N. Rapid Liquid-Phase Microextraction of Analytes
32
33 from Complex Samples on Superwetting Porous Silicon for Onsite SALDI-MS Analysis.
34
35 *Talanta* **2019**, *198*, 63–70. <https://doi.org/10.1016/j.talanta.2019.01.051>.
36
37
38 (26) Yang, Z.; Li, W.; Huang, H.; Ren, S.; Men, Y.; Li, F.; Yu, X.; Luo, Q. Detection of Serum
39
40 Phospholipids by Microchannel-Integrated Black Phosphorus-Assisted Laser
41
42 Desorption/Ionization Mass Spectrometry. *Talanta* **2022**, *237*, 122978.
43
44 <https://doi.org/10.1016/j.talanta.2021.122978>.
45
46
47 (27) Gao, X.; Bi, X.; Wei, J.; Peng, Z.; Liu, H.; Jiang, Y.; Wei, W.; Cai, Z. N-Phosphorylation
48
49 Labeling for Analysis of Twenty Natural Amino Acids and Small Peptides by Using
50
51 Matrix-Assisted Laser Desorption/Ionization Time-of-Flight Mass Spectrometry. *The*
52
53 *Analyst* **2013**, *138* (9), 2632. <https://doi.org/10.1039/c3an00036b>.
54
55
56 (28) Lecot, S.; Chevlot, Y.; Phaner-Goutorbe, M.; Yeromonahos, C. Impact of Silane
57
58 Monolayers on the Adsorption of Streptavidin on Silica and Its Subsequent Interactions
59
60

- 1
2
3 with Biotin: Molecular Dynamics and Steered Molecular Dynamics Simulations. *J. Phys.*
4
5 *Chem. B* **2020**, *124* (31), 6786–6796. <https://doi.org/10.1021/acs.jpcc.0c04382>.
6
7
8 (29) Lecot, S.; Chevlot, Y.; Phaner-Goutorbe, M.; Yeromonahos, C. Curious Binding Energy
9
10 Increase between the Receptor-Binding Domain of the SARS-CoV-2 Spike Protein and
11
12 Angiotensin-Converting Enzyme 2 Adsorbed on a Silane Monolayer from Molecular
13
14 Dynamics Simulations. *J. Phys. Chem. B* **2021**, *125* (39), 11078–11090.
15
16 <https://doi.org/10.1021/acs.jpcc.1c06050>.
17
18
19 (30) Lecot, S.; Lavigne, A.; Yang, Z.; Géhin, T.; Botella, C.; Jousseume, V.; Chevlot, Y.;
20
21 Phaner-Goutorbe, M.; Yeromonahos, C. Arrangement of Monofunctional Silane
22
23 Molecules on Silica Surfaces: Influence of Alkyl Chain Length, Head-Group Charge, and
24
25 Surface Coverage, from Molecular Dynamics Simulations, X-Ray Photoelectron
26
27 Spectroscopy, and Fourier Transform Infrared Spectroscopy. *J. Phys. Chem. C* **2020**, *124*
28
29 (37), 20125–20134. <https://doi.org/10.1021/acs.jpcc.0c05349>.
30
31
32
33 (31) Lecot, S.; Lavigne, A.; Yang, Z.; Chevlot, Y.; Phaner-Goutorbe, M.; Yeromonahos, C.
34
35 Effects of the Chemical and Structural Properties of Silane Monolayers on the
36
37 Organization of Water Molecules and Ions at Interfaces, from Molecular Dynamics
38
39 Simulations. *Langmuir* **2021**, *37* (18), 5563–5572.
40
41 <https://doi.org/10.1021/acs.langmuir.1c00338>.
42
43
44 (32) Wang, L.; Schubert, U. S.; Hoepfner, S. Surface Chemical Reactions on Self-Assembled
45
46 Silane Based Monolayers. *Chem. Soc. Rev.* **2021**, *50* (11), 6507–6540.
47
48 <https://doi.org/10.1039/D0CS01220C>.
49
50
51 (33) Iakab, S. A.; Rafols, P.; García-Altare, M.; Yanes, O.; Correig, X. Silicon-Based Laser
52
53 Desorption Ionization Mass Spectrometry for the Analysis of Biomolecules: A Progress
54
55 Report. *Adv. Funct. Mater.* **2019**, *29* (45), 1903609.
56
57 <https://doi.org/10.1002/adfm.201903609>.
58
59
60

- 1
2
3 (34) Alhmoud, H. Z.; Guinan, T. M.; Elnathan, R.; Kobus, H.; Voelcker, N. H. Surface-
4 Assisted Laser Desorption/Ionization Mass Spectrometry Using Ordered Silicon
5 Nanopillar Arrays. *The Analyst* **2014**, *139* (22), 5999–6009.
6
7 <https://doi.org/10.1039/C4AN01391C>.
8
9
10
11
12 (35) Park, J.-M.; Noh, J.-Y.; Kim, M.-J.; Yun, T. G.; Lee, S.-G.; Chung, K. S.; Lee, E. H.; Shin,
13 M. H.; Ku, N. S.; Yoon, S.; Kang, M.-J.; Park, M. S.; Pyun, J.-C. MALDI-TOF Mass
14 Spectrometry Based on Parylene-Matrix Chip for the Analysis of
15 Lysophosphatidylcholine in Sepsis Patient Sera. *Anal. Chem.* **2019**, *91* (22), 14719–
16 14727. <https://doi.org/10.1021/acs.analchem.9b04019>.
17
18
19
20
21
22
23 (36) Chughtai, K.; Jiang, L.; Greenwood, T. R.; Glunde, K.; Heeren, R. M. A. Mass
24 Spectrometry Images Acylcarnitines, Phosphatidylcholines, and Sphingomyelin in MDA-
25 MB-231 Breast Tumor Models. *J. Lipid Res.* **2013**, *54* (2), 333–344.
26
27 <https://doi.org/10.1194/jlr.M027961>.
28
29
30
31
32 (37) Pulfer, M.; Murphy, R. C. Electrospray Mass Spectrometry of Phospholipids. *Mass*
33 *Spectrom. Rev.* **2003**, *22* (5), 332–364. <https://doi.org/10.1002/mas.10061>.
34
35
36
37 (38) Drobnik, W.; Liebisch, G.; Audebert, F.-X.; Fröhlich, D.; Glück, T.; Vogel, P.; Rothe, G.;
38 Schmitz, G. Plasma Ceramide and Lysophosphatidylcholine Inversely Correlate with
39 Mortality in Sepsis Patients. *J. Lipid Res.* **2003**, *44* (4), 754–761.
40
41 <https://doi.org/10.1194/jlr.M200401-JLR200>.
42
43
44
45
46
47
48
49

50 ASSOCIATED CONTENT

51
52 The following files are available free of charge.

53
54
55
56
57 **Figure S1:** Normalized DIOS mass spectra in RP ion mode of the CH₃ short and CH₃ long
58 monolayers on porous silicon, and the bare porous silicon surface.; **Figure S2:** Normalized
59
60

1
2
3 DIOS mass spectra in RN ion mode of the CH₃ short and CH₃ long monolayers on porous
4 silicon, and the bare porous silicon surface.; **Figure S3**: DIOS mass spectra of 10 % of a mix
5 of chloroform/methanol (2/1 v:v) on bare porous silicon in RN and RP ion modes.; **Figure S4**:
6 Normalized intensities of the different fragments of LysoPC, detected in the spiked plasma
7 sample, on the CH₃ short monolayer, in RN ion mode, for different water washing protocols
8 (no washing, 1x1, 3x1, 10x1); **Figure S5**: Normalized intensities of the different fragments of
9 LysoPC, detected in the spiked plasma sample, on the CH₃ short monolayer, in RN ion mode,
10 for the different water washing protocols (10x1, 5x2, 2x5).; **Figure S6**: Normalized intensities
11 of the different fragments of LysoPC, detected in the spiked plasma sample, on the CH₃ short
12 monolayer, in RN ion mode, for the different water washing protocols (2x5, 3x5, 5x5).; **Figure**
13 **S7**: ToF-SIMS depth profiling of porous silicon functionalized by CH₃ short monolayer, after
14 LysoPC adsorption, with (red) and without (black) water washings. The intensities of the P⁻
15 ions (30.9682 amu) and ³⁰Si⁻ (29.9717 amu) ions as a function of sputtering are displayed.

16
17
18
19
20
21
22
23
24
25
26
27
28
29
30
31
32
33 (PDF)

34 35 36 AUTHOR INFORMATION

37 38 39 **Corresponding Author**

40
41
42 *Email: christelle.yeromonahos@ec-lyon.fr

43 44 45 **Author Contributions**

46
47
48 The manuscript was written through contributions of all authors. All authors have given
49 approval to the final version of the manuscript.

50 51 52 **Funding Sources**

53
54
55 This work was supported by the Young Researcher ANR PORIDG project, grant ANR-18-
56 CE09-0006 of the French Agence Nationale de la Recherche.

1
2
3 ACKNOWLEDGMENT
4
5

6 A. L. is grateful to the ANR PORIDG, of the French Agence Nationale de la Recherche, for
7
8 funding his Ph.D. fellowship.
9
10
11
12
13
14
15
16
17
18
19
20
21
22
23
24
25
26
27
28
29
30
31
32
33
34
35
36
37
38
39
40
41
42
43
44
45
46
47
48
49
50
51
52
53
54
55
56
57
58
59
60

1
2
3
4
5
6
7
8
9
10
11
12
13
14
15
16
17
18
19
20
21
22
23
24
25
26
27
28
29
30
31
32
33
34
35
36
37
38
39
40
41
42
43
44
45
46
47
48
49
50
51
52
53
54
55
56
57
58
59
60